Modeling and multi-objective optimization of the digestion tank of an industrial process for manufacturing phosphoric acid by wet process

Ilias Bouchkira, Abderrazak Latifi, Lhachmi Khamar, Saad Benjelloun

Modeling and multi-objective optimization of the digestion tank of an industrial process for manufacturing phosphoric acid by wet process

Ilias Bouchkira[a,b,c], Abderrazak M. Latifi[a,b,*], Lhachmi Khamar[a,d], Saad Benjelloun[b]

[a]*Laboratoire Réactions et Génie des Procédés, CNRS-ENSIC, Université de Lorraine, Nancy Cedex, France*
[b]*Mohammed VI Polytechnic University, Lot 990 Hay Moulay Rachid, Benguerir, Morocco*
[c]*Laboratory of Physical-Chemistry, Catalysis Environment, University Hassan II-Casablanca, Casablanca, Morocco*
[d]*Laboratoire d'Ingénierie des Procédés, Informatique et Mathématiques, Université Sultan Moulay Slimane, Beni-Mellal, Morocco*

Abstract

This paper deals with the modeling and multi-objective optimization of an industrial phosphoric acid process. The objective is to determine the operating conditions which minimize the chemical losses of phosphate and maximize the productivity of the digestion tank. To achieve these objectives, a process model, based on mass, charge, and energy balances along with thermodynamic equilibrium equations is developed. Experimental measurements concerning sulfur and phosphorus based systems are carried out and other measurements concerning fluorine, silica and calcium sulfates based systems are collected from the literature. The results show that the predictions are in very good agreement with the measurements. The developed model is then used in a multi-objective optimization problem of an industrial manufacturing process to determine the set of optimal operating conditions. The optimization problem is solved by means of epsilon-constraint method and the optimal solutions are ranked using the multi-attribute utility theory. The best solutions are compared to industrial measurements based on surrogate modeling and are found to be very consistent with the current operating conditions. Their implementation would significantly improve the current process performances.

Keywords: Phosphoric acid process, Digestion tank, Modeling, Multi-objective optimization, Surrogate model, Decision making.

1. Introduction

Phosphoric acid is one of the most produced and marketed chemicals in the world. It is mainly used in the manufacture of fertilizers (Leikam and Achorn, 2005; Li et al., 2016; Rickard, 2000), in the food industry (Amin et al., 2010; Lampila, 2013) and even in the pharmaceutical industry (Geeson and Cummins, 2018). In several producing countries, it is produced by the wet process which consists of reacting the phosphate ore with sulfuric acid (Becker, 1989; Dorozhkin, 1996; Slack, 1968; Slack and James, 1973).

*Corresponding author
Email address: abderrazak.latifi@univ-lorraine.fr (Abderrazak M. Latifi)

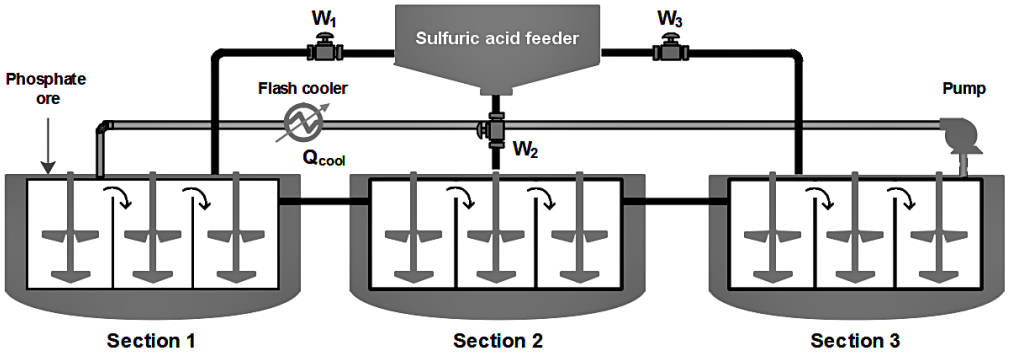

Figure 1: Schematic representation of an industrial wet phosphoric acid process

On industrial scale, phosphoric acid is mainly produced by the digestion of the phosphate ore using a concentrated sulfuric acid solution. The digestion is carried out in a cylindrical tank which consists of a series of nine continuous reactors of the same volume and uniformly distributed inside the tank. The latter is further divided into three sections of three continuous reactors each. The sulfuric acid feed flow rate is therefore split into three streams, each feeding one of the three sections. The phosphate ore is fed into the first reactor of the first section and the final product leaves the tank at the last reactor of the third section (Fig. 1).

During the digestion process, as shown by the overall reaction below, sulfuric acid is dissociated into H^+ and SO_4^{2-} ions. The H^+ ions are involved in the extraction of the phosphate elements and their diffusion from the solid phase (phosphate ore) towards the liquid phase (phosphoric acid) whereas the SO_4^{2-} ions crystallize with the calcium ions Ca^{2+} to form a solid calcium sulfate which can be either anhydrite $CaSO_4$, gypsum $CaSO_4{:}2H_2O$ or bassanite $CaSO_4{:}0.5H_2O$ depending on the operating conditions, in particular, the temperature and the sulfates concentration (Becker, 1989; Dorozhkin, 1996; Slack, 1968; Slack and James, 1973). The liquid phosphoric acid and solid calcium sulfates are separated in a vacuum filtration unit downstream. Phosphoric acid is recovered for valorization and marketing, while solid calcium sulfates are eliminated as an undesirable product.

$$\mathrm{Ca_3(PO_4)_2} + 3\,\mathrm{H_2SO_4} + y\,\mathrm{H_2O} \longrightarrow 2\,\mathrm{H_3PO_4} + 3\,\mathrm{CaSO_4}, x\,\mathrm{H_2O}; \qquad x \in \{0, 0.5, 2\}$$

Moreover, the production of more gypsum enhances the productivity by increasing the phosphoric acid production, whereas the production of the bassanite increases the viscosity of the reactive mixture within the reactors and consequently lowers the performances of the filtration process downstream. It is therefore very important to control the operating conditions to favor the production of gypsum and limit the formation of the bassanite.

On the other hand, the required amount of sulfuric acid should be optimally used in order to optimize the production performances. Indeed, a deficit in sulfuric acid during the digestion causes a decrease in sulfate ions SO_4^{2-} concentration in the digestion tank. Therefore, the free calcium ions (coming from the raw rock) tend to capture the phosphate ions HPO_4^{2-} and crystallize them as solid brushite $CaHPO_4{:}2H_2O$. The latter decreases the chemical yield of the process since the solid phase is discharged as undesirable product leading to phosphate losses by syncrystallization (Becker, 1989; Slack, 1968). On the contrary, the use of an excess of sulfuric acid causes

not only a local increase of the temperature due to the heat of dilution, but also leads to the formation of a gypsum layer around the phosphate particles (particle coating) thus protecting them from further attack by the sulfuric acid and resulting also in phosphate losses (unattacked losses). The appropriate amount of sulfuric acid along with its optimal distribution over the three sections of the digestion tank are then relevant to the optimal operation of the digestion tank.

In this paper, the objective is to determine the operating conditions of the digestion tank that minimize the phosphate ore losses (syncrystallized and unattacked) while meeting the constraints on the excess of sulfuric acid above the stoechiometric amount and on the reaction temperature. Beforehand, Pitzer's thermodynamic model, needed in optimization, is calibrated using experimental measurements.

2. Optimization problem formulation

A multi-objective optimization problem is formulated and solved in this work in order to determine the trade-offs between the following objectives: (i) limit the syncrystallized losses by minimizing the precipitation of the solid brushite, (ii) enhance the productivity of the process by maximizing the production of gypsum, (iii) limit the unattacked losses by setting the excess of sulfuric acid over the stoichiometric amount between two limit values that ensure the optimal operation of the process, (iv) control the temperature of the reaction in order to limit the production of the bassanite and thus improve the filtration downstream of the process.

The first two objectives are taken into account by means of two criteria, whereas, the remaining two objectives are considered as constraints. The ingredients of the multi-objective optimization problem considered are presented in the next section.

2.1. Objective functions

The two (conflicting) optimization criteria are defined by the saturation index (Chidambaram et al., 2011) of the brushite to be minimized all over the sections of the process to limit its production, and the saturation index of gypsum to be maximized to enhance the process productivity. These two criteria are expressed as:

$$f_1 = \frac{1}{3} \sum_j log\left(a_{Ca^{2+}}.a_{HPO_4^{2-}}.a_{H_2O}^2.k_{s_1}^{-1}\right)^j \tag{1}$$

$$f_2 = \frac{1}{3} \sum_j log\left(a_{Ca^{2+}}.a_{SO_4^{2-}}.a_{H_2O}^2.k_{s_2}^{-1}\right)^j \tag{2}$$

where a_i is the activity of component i in the reaction mixture, k_{s_1} and k_{s_2} are the solubility products of the brushite and of the gypsum respectively and, j refers to the number of each section.

2.2. Decision variables

The decision variables consist of the excess of sulfuric acid S_c over the stoichiometric amount required by the reactions, its distribution ratios over the sections, i.e., w_1, w_2 and w_3, and the cooling heat Q_{cool} to be evacuated to control the temperature of the reaction (Fig. 1).

2.3. Equality and inequality constraints

Two inequality constraints are introduced to account for the last two objectives. The first one sets the lower and upper limits of sulfuric acid excess to specific values which minimize the unattacked losses. These limits correspond to 1 % and 3 % (Becker, 1989). The second inequality constraint addresses the operating temperature that should remain below 355 K to avoid the production of the solid bassanite. These inequality constraints are expressed as :

$$1\ \% \leq S_c \leq 3\ \% \tag{3}$$

$$T \leq 355\ K \tag{4}$$

The equality constraints consist of process model equations which are based on mass balance (Eqs.(5)), charge balance (Eq.(6)), equilibrium constants equations (Eqs.(7-8)), and finally heat balance (Eq.(10)).

$$(M)^{tot} = \sum_{i=1}^{N_C} \delta_{M,i} m_i, \qquad M \in \{S, P, F, Si, Ca\} \tag{5}$$

$$\sum_{i=1}^{N_C} z_i.m_i = 0 \tag{6}$$

$$K_j = \prod_{i=1}^{N_C} a_i^{\alpha_{ij}} = \prod_{i=1}^{N_C} (m_i.\gamma_i)^{\alpha_{ij}}, \qquad j = 1, .., N_R \tag{7}$$

$$log(K_j) = log(K_{j0}) + \frac{\Delta H_j}{R}\left(\frac{1}{T} - \frac{1}{T_0}\right) \tag{8}$$

where N_C is the number of components, N_R corresponds to the number of reactions, $(M)^{tot}$ is the total concentration of M. m_i is the molality of each component i involved in the equilibria in Table 1, $\delta_{M,i}$ is the number of element M in component i. For example, for phosphorus element $\delta_{P,H_5P_2O_8^-} = 2$.

As an exemple, the mass balance on (P) develops as:

$$(P)^{tot} = m_{H_3PO_4} + m_{H_2PO_4^-} + m_{HPO_4^{2-}} + 2.m_{H_5P_2O_8^-} \tag{9}$$

z_i are the electrical charges, γ_i and a_i are the activity coefficient and the activity of component i respectively. α_{ij} is the stoichiometric coefficient of component i involved in reaction j. K_{j0} and ΔH_j refer to the equilibrium constant and the enthalpy of the reaction j at $T_0 = 298\ K$ respectively, their values are reported in Table 1.

Table 1: Reactions involved in the digestion tank and their corresponding equilibrium constant and enthalpy at 298K.

	Equilibria	K_{j0}	$\Delta H_j(J/moles)$	Database
1	$H_2SO_4 \longrightarrow HSO_4^- + H^+$	-	-	-
2	$HSO_4^- \overset{K1}{\rightleftharpoons} SO_4^{2-} + H^+$	0.0103	$-1.2.10^4$	Gustafsson (2011) ; Pitzer (2018)
3	$H_3PO_4 \overset{K2}{\rightleftharpoons} H_2PO_4^- + H^+$	0.0071	$-4.2.10^3$	Gustafsson (2011)
4	$H_2PO_4^- \overset{K3}{\rightleftharpoons} HPO_4^{2-} + H^+$	$4.2.10^{-12}$	$-1.5.10^4$	Gustafsson (2011)
5	$H_2PO_4^- + H_3PO_4 \overset{K4}{\rightleftharpoons} H_5P_2O_8^-$	0.2550	$-9.2.10^3$	Gustafsson (2011)
6	$HF \overset{K5}{\rightleftharpoons} F^- + H^+$	$7.2.10^{-4}$	$-1.3.10^4$	Ball and Nordstrom (1991)
7	$HF + F^- \overset{K6}{\rightleftharpoons} HF_2^-$	5.5000	$-1.7.10^4$	Ball and Nordstrom (1991)
8	$H_2SiF_6 \overset{K7}{\rightleftharpoons} SiF^{2-} + 2\,H^+$	$0.3.10^2$	$-6.7.10^4$	Gustafsson (2011)
9	$Ca^{2+} + SO_4^{2-} \overset{K8}{\rightleftharpoons} CaSO_4$	0.6394	$-7.2.10^3$	Gustafsson (2011) ; Pitzer (2018)

Finally, the heat balance for each section of the process is expressed as (Fig. 2) :

$$Q_H + Q_{AG} + Q_{R+D} = Q_{cool} + Q_{out} + Q_{loss} \tag{10}$$

where Q_H, Q_{AG}, Q_{R+D}, Q_{out}, Q_{loss} and Q_{cool} refer respectively to the enthalpy of the inlet reactants, the agitation heat, the sulfuric acid dilution heat, the enthalpy of the slurry leaving the reactor, the heat losses of the digestion tank and the heat to be removed to control the temperature. The enthalpy of the inlet and outlet streams are expressed as follows:

$$Q_H = Q_{sa} + Q_{ps} + Q_{rph} \tag{11}$$

$$Q_{out} = V_{out}\rho_{out}C_{p_{out}}(T_{out} - T_0) \tag{12}$$

where :

$$Q_{sa} = m_{sa}C_{p_{sa}}(T_{sa} - T_0) \tag{13}$$

$$Q_{ps} = V_{ps}\rho_{ps}C_{p_{ps}}(T_{ps} - T_0) \tag{14}$$

$$Q_{rph} = V_{rph}\rho_{rph}C_{p_{rph}}(T_{rph} - T_0) \tag{15}$$

m_{sa}, $C_{p_{sa}}$, T_{sa} are the mass flow rate, the heat capacity and the temperature of sulfuric acid respectively.V_{ps}, $C_{p_{ps}}$, ρ_{ps}, T_p are the volume flow rate, the heat capacity, the density and the temperature of the phosphate slurry respectively. V_{rph}, $C_{p_{rph}}$, ρ_{ph}, T_{rph} are the volume flow rate, the heat capacity, the density and the temperature of the recycled phosphoric acid respectively. V_{out}, $C_{p_{out}}$, ρ_{out}, T_{out} are the volume flow rate, the heat capacity, the density and the temperature of the outlet flow respectively. T_0 is the reference temperature. It is worth mentioning that the correlations developed by Becker (1989) are used to estimate the agitation heat and the heat released by the dilution of sulfuric acid. It should be noted that Q_{loss} is greater for small units than for large ones due to their large surface/volume ratio. Its value is often too low to be taken into account and is therefore neglected.

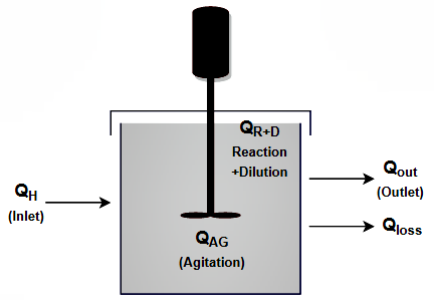

Figure 2: Heat balance in a single reactor of a section in the digestion tank

2.4. Pitzer's thermodynamic model

Pitzer's thermodynamic model (Pitzer, 2018) is widely used to describe the interactions between dissolved ions and the solvent. Its use depends mainly on the chemical species present in solution. The general expression of this model provides the excess Gibbs energy for a solution containing n_w kg of solvent through the following relation:

$$\frac{G^{ex}}{W_n RT} = n_w f + \sum_{i,j} m_i m_j \lambda_{i,j} + \sum_{i,j,k} m_i m_j \psi_{i,j,k} + ... \tag{16}$$

$\lambda_{i,j}$ represents the short-distance binary interactions between solute species i and j. $\psi_{i,j,k}$ represents the ternary interaction parameters. R is the perfect gas constant,W_n is the mass of the solvant, T is the temperature, f is the Debye-Huckel function (Pitzer, 2018) which depends on the ionic strength I as:

$$f = -\frac{4A_\phi I}{b} ln\left(1 + I^{0.5}\right) \tag{17}$$

$$A_\phi = \frac{1}{3}(2\pi N_0 d_w/1000)^{\frac{1}{2}}(e^2 DkT)^{\frac{3}{2}} \tag{18}$$

where A_ϕ is the Debye-Huckel constant, b is a characteristic constant. N_0 is the Avogadro number, d_w is the density of water, D is the dielectric constant of water at temperature T, k is Boltzmann's constant and e is the electrical charge. The activity coefficient γ_i is given by the Pitzer model as (Pitzer, 2018):

$$ln(\gamma_i) = \frac{z_i^2}{2} f + 2\sum_j m_j \lambda_{i,j}(I) + z_i^2 \sum_j m_j m_k \lambda'_{j,k}(I) + 3\sum_{j,k} m_i m_j m_k \psi_{i,j,k} + ... \tag{19}$$

where:

$$I = \frac{1}{2}\sum_i m_i z_i^2, \quad \lambda'_{i,j} = \frac{d\lambda_{i,j}}{dI}, \quad m_i = \frac{n_i}{n_w} \tag{20}$$

Pitzer gives more appropriate forms of his theory by using $\beta_{i,j}$ to express the parameters $\lambda_{i,j}$ and $\lambda'_{i,j}$. Moreover, these parameters are temperature dependent (Simoes et al., 2017) and are usually expressed as (Eqs. 21-25).

$$\lambda_{i,j}(I) = \beta^{(0)}_{i,j} + \beta^{(1)}_{i,j} \frac{2}{b}\left[1 - (1 + \alpha\sqrt{I})e^{-\alpha\sqrt{I}}\right] \tag{21}$$

$$\lambda^{'}_{i,j}(I) = \frac{\beta^{(1)}_{i,j}}{\alpha^2 I}\left[-1 + (1 + \alpha\sqrt{I} + \alpha I)e^{-\alpha\sqrt{I}}\right] \tag{22}$$

where:

$$\beta^{(0)}_{i,j}(T) = a^{(0)}_{i,j} + b^{(0)}_{i,j}.(T - T_0) + \frac{c^{(0)}_{i,j}}{T - T_0} \tag{23}$$

$$\beta^{(1)}_{i,j}(T) = a^{(1)}_{i,j} + b^{(1)}_{i,j}.(T - T_0) + \frac{c^{(1)}_{i,j}}{T - T_0} \tag{24}$$

$$\psi_{i,j,k}(T) = a^{(2)}_{i,j,k} + b^{(2)}_{i,j,k}.(T - T_0) + \frac{c^{(2)}_{i,j,k}}{T - T_0} \tag{25}$$

Therefore, the Pitzer model involves several binary and ternary interaction parameters that must be identified from experimental measurements. However, an important question that always arises is to know whether the available data allow to identify all the model unknown parameters or only a subset of them. To answer this question, a database of experimental measurements as well as an estimability analysis of the unknown parameters are presented in the next section.

3. Experimental database and parameter identification

The identification of the unknown parameters of the thermodynamic model requires experimental measurements of the most important variables. In this work, experimental measurements concerning sulfuric and phosphoric acid systems have been carried out in the laboratory, whereas data concerning other thermodynamic systems were collected from the literature (Table 2).

3.1. Laboratory measurements

Different series of experimental measurements of sulfuric and phosphoric acid solutions have been carried out. They consist of pH, density, electrical conductivity and molalities of the ionic and molecular species considered. These measurements were carried out as follows: (i) the pH is measured by means of a glass electrode pH meter, calibrated using a KCl solution at different temperatures, (ii) a pycnometer of known volume and mass is used to measure the density of the samples, (iii) the total concentrations of the ions and molecules present in the acid solutions are calculated using a conductivity based method developed by McCleskey et al. (2012) for the case of sulfuric acid, and a pH based method developed by Elmore et al. (1965) for the case of phosphoric acid.

For all the experiments, 98$w\%$ sulfuric acid and 65$w\%$ phosphoric acid were used to prepare several samples. The temperature and the concentration of the samples varied respectively from 298K and 353K and from infinite dilution to 4$moles/kgw$ for sulfuric acid and from infinite dilution to 16$moles/kgw$ for phosphoric acid.

Table 2: Recent experimental measurements from the literature for the identification of the unknown model parameters and the validation of the models results. Molality is expressed in ($moles/kgw$) and temperature in (K).

System	Type of data	Molality	Temperature	Reference
$H_3PO_4 - H_2O$	Osmotic coefficient	0–10.0	298-373	Messnaoui and Bounahmidi (2005)
	&	0–9.00	298	Cherif et al. (2000)
	Speciation	0-18.0	298	Yang et al. (2016)
		0-7.00	298-540	Holmes and Mesmer (1999)
		0-4.37	283-353	Preston and Adams (1979)
$H_2SO_4 - H_2O$	Osmotic coefficient	0-6.00	298-328	Sippola and Taskinen (2014)
	&	0-4.00	298	Messnaoui and Bounahmidi (2006)
	Speciation	0-6.00	298	Christov and Moller (2004)
		0-23.5	298	Irish and Chen (1971)
		0-6.00	298-373	Wang et al. (2013)
		0-6.00	298-473	Sippola (2012)
$CaSO_4 : 2H_2O - H_2SO_4$	Gypsum solubility	0-4.0	298-363	Wang et al. (2013)
		0-0.49	298-363	Azimi and Papangelakis (2010)
		0-0.79	303-353	Dutrizac (2002)
		0-4.70	298-333	Shen et al. (2020)
		0-6.84	283-368	Zdanovskii and Vlasov (1968)
$CaSO_4 - H_2SO_4$	Anidrhyte solubility	0-4.65	298-363	Wang et al. (2013)
		0-0.79	363-378	Dutrizac (2002)
		0-1.20	398-368	Shen et al. (2020)
		0-4.37	283-323	Zdanovskii and Vlasov (1968)
$HF - H_2O$	Water activity	0-6.00	298-353	El Guendouzi et al. (2019)
		0-6.00	298	Braddy et al. (1994)
$H_2SiF_6 - H_2O$	Water activity	0-3.00	298-353	El Guendouzi et al. (2015)

3.2. Estimability and identification of the model parameters

The estimability of the unknown parameters of Pitzer's model is carried out using our recently developed method (Bouchkira et al., 2021) based on the matrix of global sensitivities. The most estimable parameters are then identified from the available measurements using an optimization method based on the branch-and-reduce algorithm developed by (Belotti et al., 2009; Sahinidis, 2002), to minimize the following mean-square-error objective function to global optimality:

$$J^{mse} = \sum_{k} \sum_{T} \sum_{m} \left(\frac{k^{exp}_{m,T} - k^{mod}_{m,T}}{\omega_k} \right)^2 \tag{26}$$

k corresponds to the measured variables, i.e., water activity, component molalities and solubility, ω_i are weighting factors, T and m refer to the temperature and total concentrations. The accuracy of identification is assessed by means of confidence intervals (Langman, 1986). Assuming that the objective function can be expressed in the following form:

$$F(P) = \theta(P)^T . W . \theta(P) \tag{27}$$

$\theta(P)$ is the residual vector, i.e., the difference between the model predictions and the measured values of the outputs, W is a weighting matrix (equal to the identity, since we assume that all measurements have the same weight in the objective function), and P is the vector of the unknown parameters. Assuming that the measurement errors are independent and normally distributed, the covariance matrix C of the least square problem is approximated as follows (Langman, 1986):

$$C \approx \frac{F(P^*)}{d-n}(J^T J)^{-1} J^T J (J^T J)^{-1} \tag{28}$$

P^* is the vector of parameters that minimizes the objective function $F(P)$, J is the Jacobian matrix of the vector $\theta(P)$. This approximation is more accurate when the non-linearities are not strong.

The Jacobian matrix is computed using a local "One-At-Time" (OAT) method. It consists in perturbing the value of each parameter P_j^* by 10% forward and backward, then, the centered finite difference method is used to approximate the elements of J.

$$J = \begin{pmatrix} \frac{\partial \theta_1}{\partial P_1} & \cdots & \frac{\partial \theta_1}{\partial P_{np}} \\ \vdots & \ddots & \vdots \\ \frac{\partial \theta_{ny}}{\partial P_1} & \cdots & \frac{\partial \theta_{ny}}{\partial P_{np}} \end{pmatrix}$$

ny and np correspond respectively to the number of outputs and the number of unknown parameters. The uncertainty on a parameter j is calculated as follows:

$$\epsilon_{P_j} = \pm \frac{\sqrt{c_{jj}} t_{1-\alpha/2,\nu}}{P_j^*}.100\% \tag{29}$$

c_{jj} is the j^{th} diagonal element of the C matrix. $t_{1-\alpha/2,\nu}$ is deduced from the Student table with ν degrees of freedom, it corresponds to the probability of $1-\alpha/2$ that the true value of the parameter is within the confidence interval given by:

$$P_j \in \left[P_j^* - \sqrt{c_{jj}} t_{1-\alpha/2,\nu}; P_j^* + \sqrt{c_{jj}} t_{1-\alpha/2,\nu} \right] \tag{30}$$

On the other hand, the quality of the model predictions with respect to the experimental measurements is quantified using the Pearson correlation coefficient (Keith, 2014), given as :

$$r = \frac{\sum_{i,j} \left(S_{ij}^m - \overline{S_{ij}^m} \right) \left(S_{ij}^e - \overline{S_{ij}^e} \right)}{\sqrt{\left(\sum_{i,j} (S_{ij}^m - \overline{S_{ij}^m}) \right)^2 \left(\sum_{i,j} (S_{ij}^e - \overline{S_{ij}^e}) \right)^2}} \tag{31}$$

where S_{ij}^m is the model prediction, S_{ij}^e is the corresponding experimental value and $\overline{S_{ij}}$ is their average over the total number of available measurements performed at different molalities and temperatures. The indices i and j refer to molalities and temperatures respectively.

Table 3: Interaction parameters along with their confidence intervals. (A): sulfur, (B): phosphorus acid, (C): fluorine, (D): silica, (E): calcium.

	a	C.I	*b*	C.I	*c*	C.I
(A)						
$\beta^{(0)}_{HSO_4^-,SO_4^{2-}}$	-2.471	[-3.00;-1.934]	0.007	[0.004;0.010]	0.01	-
$\beta^{(0)}_{HSO_4^-,H^+}$	1.046	[0.518;1.573]	-0.002	[-0.003;-0.001]	0.01	-
$\beta^{(0)}_{SO_4^{2-},H^+}$	-8.001	[-9.665;-6.336]	0.01	-	1684.0	[1221.1;2147.04]
$\beta^{(1)}_{HSO_4^-,SO_4^{2-}}$	-254.8	[-312.8;-196.8]	0.405	[0.341;0.468]	$3.9.10^4$	[$3.1.10^4$;$4.8.10^4$]
$\beta^{(1)}_{HSO_4^-,H^+}$	-296.9	[-489.1;-104.8]	0.453	[0.341;0.564]	$4.8.10^4$	[$2.7.10^4$;$7.0.10^4$]
$\beta^{(1)}_{SO_4^{2-},H^+}$	8.039	[4.879;11.19]	-0.023	[-0.032;-0.013]	0.01	-
$\psi_{H^+,HSO_4^-,SO_4^{2-}}$	1.696	[1.142;2.249]	-0.003	[-0.004;-0.001]	-277.209	[-335.9;-218.4]
(B)						
$\beta^{(0)}_{H^+,H_3PO_4}$	4.211	[3.75;4.67]	0.134	[0.12;0.15]	$2.49.10^3$	[$2.21.10^3$;$2.76.10^3$]
$\beta^{(0)}_{H^+,H_2PO_4^-}$	-2.965	[-3.32;-2.61]	-1.005	[-1.13;-0.88]	203.473	[179.06;227.89]
$\beta^{(0)}_{H^+,H_5P_2O_8^-}$	-186.465	[-242.4;-130.5]	2.203	[1.54;2.86]	0.198	[0.14;0.26]
$\beta^{(0)}_{H_3PO_4,H_2PO_4^-}$	0.183	[0.17;0.20]	-0.088	[-0.10;-0.08]	$-1.25.10^4$	[$-1.37.10^4$;$-1.14.10^4$]
$\beta^{(0)}_{H_3PO_4,H_5P_2O_8^-}$	4.739	[4.17;5.31]	-0.161	[-0.18;-0.14]	0.925	[0.81;1.04]
$\beta^{(0)}_{H_2PO_4^-,H_5P_2O_8^-}$	168.178	[126.1;210.2]	1.941	[1.46;2.43]	$4.49.10^5$	[$3.36.10^5$;$5.61.10^5$]
$\beta^{(1)}_{H^+,H_3PO_4}$	-2.495	[-3.24;-1.75]	-0.311	[-0.40;-0.22]	$-4.96.10^4$	[$-6.45.10^4$;$-3.47.10^4$]
$\beta^{(1)}_{H^+,H_2PO_4^-}$	16.109	[12.4;19.8]	1.404	[1.08;1.73]	-	-
$\beta^{(1)}_{H^+,H_5P_2O_8^-}$	56.786	[45.4;68.1]	-	-	$9.14.10^4$	[$7.31.10^4$;$1.09.10^4$]
$\beta^{(1)}_{H_3PO_4,H_2PO_4^-}$	-8.458	[-9.30;-7.61]	0.064	[0.06;0.07]	-1871.020	[-2058.12;-1683.92]
$\beta^{(1)}_{H_3PO_4,H_5P_2O_8^-}$	-3.712	[-4.19;-3.23]	-	-	$-3.05.10^4$	[$-3.44.10^4$;$-2.65.10^4$]
$\beta^{(0)}_{H_2PO_4^-,H_5P_2O_8^-}$	-4.093	[-4.91;-3.27]	0.236	[0.19;0.28]	-	-
$\psi_{H_3PO_4,H_3PO_4,H_3PO_4}$	6.826	[5.46;8.19]	-	-	-	-
$\beta^{(0)}_{H_3PO_4,H_3PO_4}$	-	-	-	-	-134.046	[-135.39;-132.71]
(C)						
$\beta^{(0)}_{H^+,HF}$	-	-	-0.007	[-0.0078;-0.0062]	-	-
$\beta^{(0)}_{HF_2^-,HF}$	0.208	[0.19;0.23]	-	-	-	-
$\beta^{(0)}_{F^-,HF}$	-	-	0.013	[0.0118;0.0142]	-	-
$\beta^{(0)}_{HF_2^-,HF}$	-0.392	[-0.44;-0.35]	.	-	-	-
$\psi_{HF,HF,HF}$	-3.081	[-4.01;-2.16]	-	-	-	-
$\beta^{(0)}_{HF,HF}$	-	-	-	-	-84.628	[-93.94;-75.32]
(D)						
$\beta^{(0)}_{H^+,H_2SiF_6}$	-	-	0.072	[0.064;0.079]	-	-
$\beta^{(0)}_{H^+,SiF_6^{2-}}$	-	-	-1.338	[-1.45;-1.21]	$-9.071.10^4$	[$-1.00.10^5$;$-8.07.10^4$]
$\beta^{(0)}_{H_2SiF_6,SiF_6^{2-}}$	12.112	[10.7;13.4]	0.077	[0.067;0.086]	-3.746	[-4.08;-3.40]
$\beta^{(1)}_{H^+,H_2SiF_6}$	-4.602	[-5.01;-4.18]	-7.095	[-8.15;-6.030]	$-7.728.10^5$	[$-8.65.10^5$;$-6.80.10^5$]
$\beta^{(1)}_{H^+,SiF_6^{2-}}$	-63.290	[-72.7;-53.7]	-	-	$-8.341.10^4$	[$-9.42.10^4$;$-7.25.10^4$]
$\beta^{(1)}_{H_2SiF_6,SiF_6^{2-}}$	-0.149	[-0.16;-0.12]	-	-	-	-
$\beta^{(0)}_{H_2SiF_6,H_2SiF_6}$	-	-	0.005	[0.004;0.0055]	-	-
$\beta^{(1)}_{H_2SiF_6,H_2SiF_6}$	-	-	0.040	[0.036;0.0436]	-	-
(E)						
$\beta^{(0)}_{HSO_4^-,CaSO_4}$	0.920	[0.81;1.02]	-0.030	[-0.033;-0.026]	-3272.216	[-3632.1;-2912.2]
$\beta^{(0)}_{HSO_4^-,Ca^{2+}}$	1.010	[0.91;1.10]	0.026	[0.023;0.028]	-	-
$\beta^{(0)}_{SO_4^{2-},CaSO_4}$	-1.801	[-2.01;-1.58]	0.010	[0.0088;0.0112]	-	-
$\beta^{(0)}_{SO_4^{2-},Ca^{2+}}$	-1.037	[-1.19;-0.88]	0.066	[0.0561;0.0759]	-1075.927	[-1194.2;-957.5]
$\beta^{(0)}_{H^+,CaSO_4}$	0.697	[0.60;0.78]	0.033	[0.028;0.037]	-	-
$\beta^{(1)}_{SO_4^{2-},Ca^{2+}}$	-	-	-	-	23487.762	[20904.1;26071.4]
$\beta^{(1)}_{H^+,CaSO_4}$	-7.917	[-8.78;-7.04]	-	-	-	-
$\beta^{(1)}_{H^+,Ca^{2+}}$	-	-	-	-	-912.578	[-1022.0;-803.0]
$\beta^{(1)}_{CaSO_4,Ca^{2+}}$	-26.026	[-28.8;-23.1]	-	-	-	-
$\psi_{CaSO_4,CaSO_4,CaSO_4}$	0.689	[0.61;0.76]	-	-	-	-

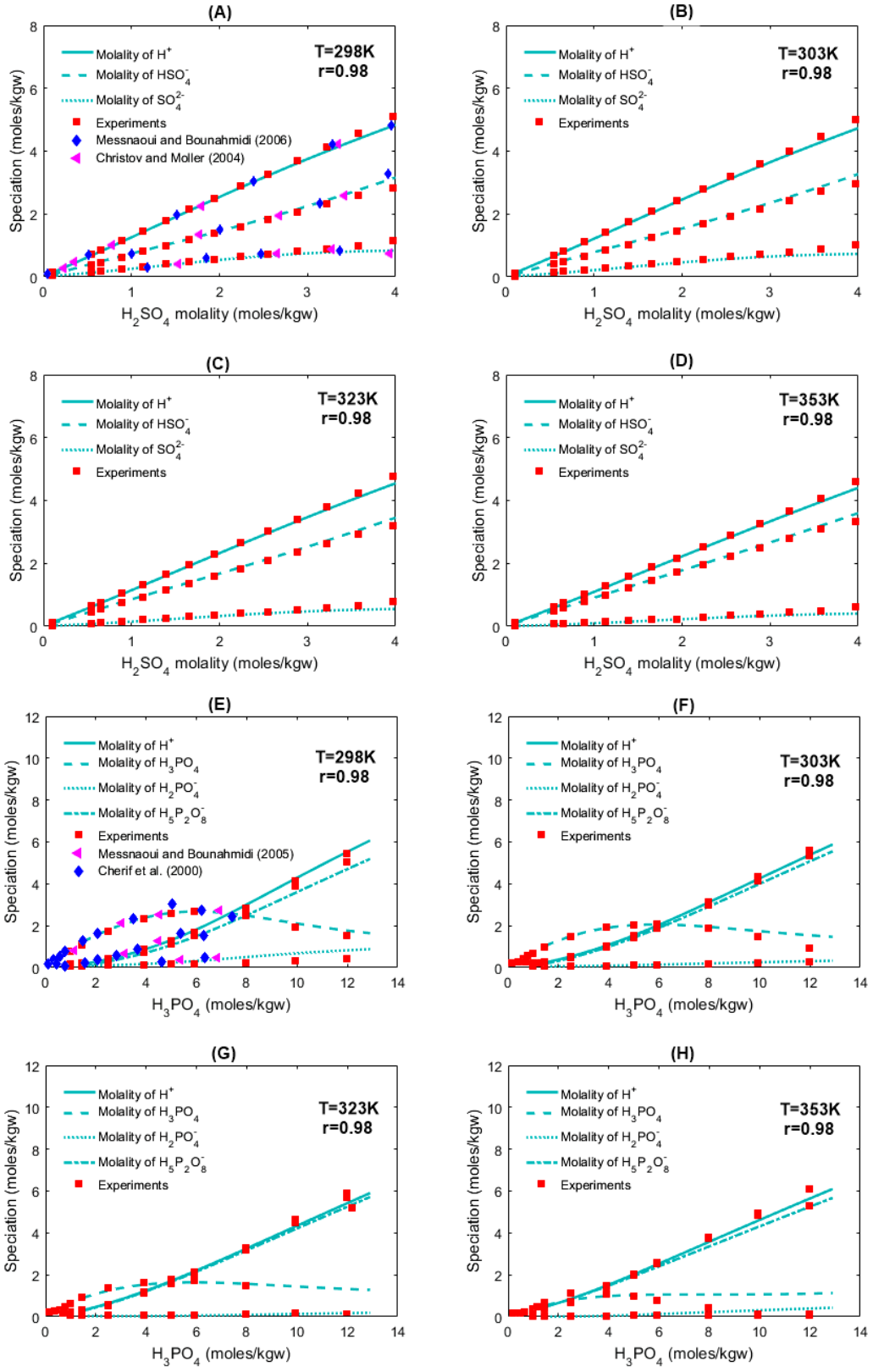

Figure 3: Model vs measurements. (A-D): speciation of sulfuric acid. (E-H): speciation of phosphoric acid.

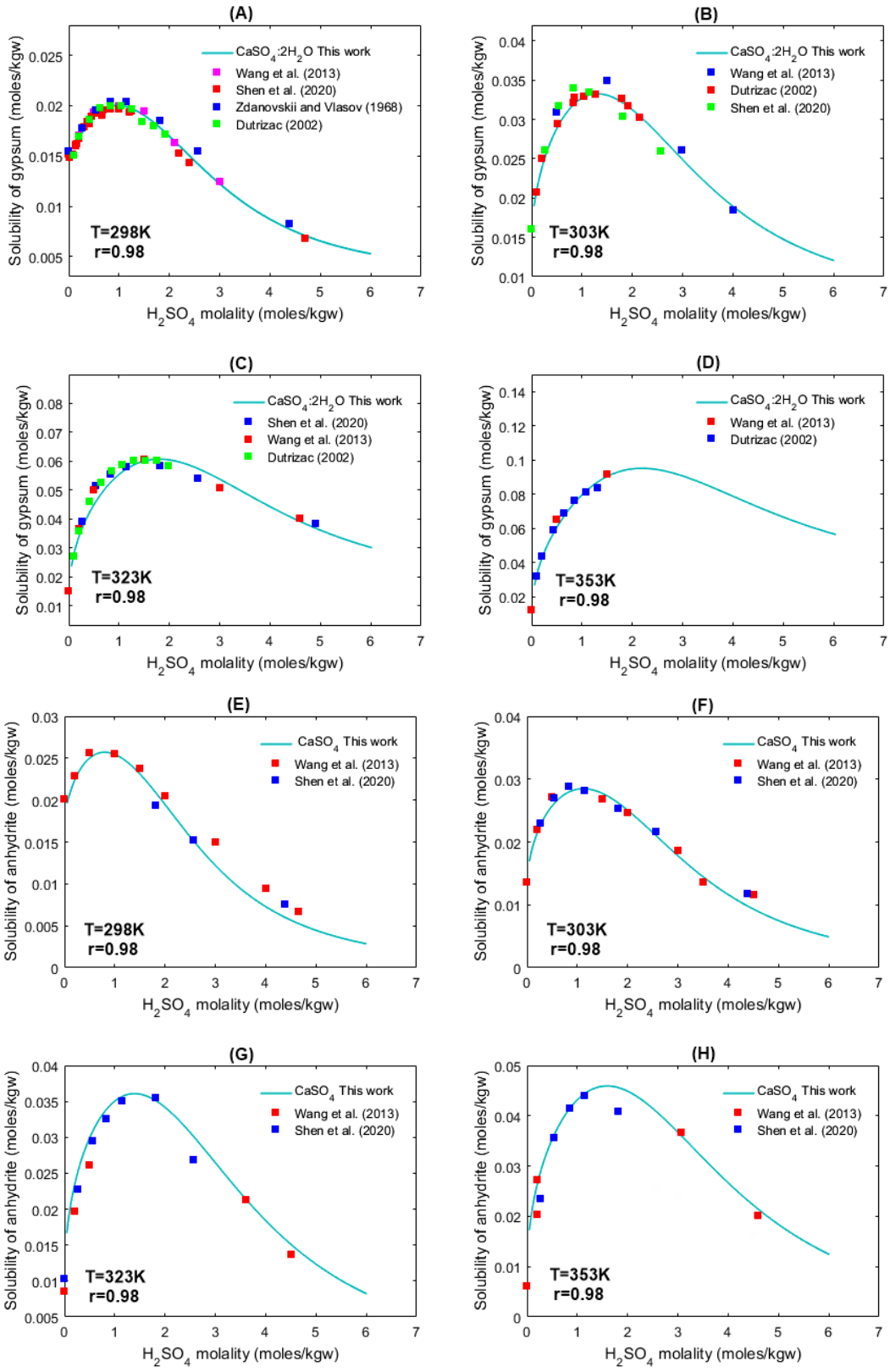

Figure 4: Model vs measurements. (A-D):gypsum solubility in sulfuric acid. (E-H): anhydrite solubility in sulfuric acid.

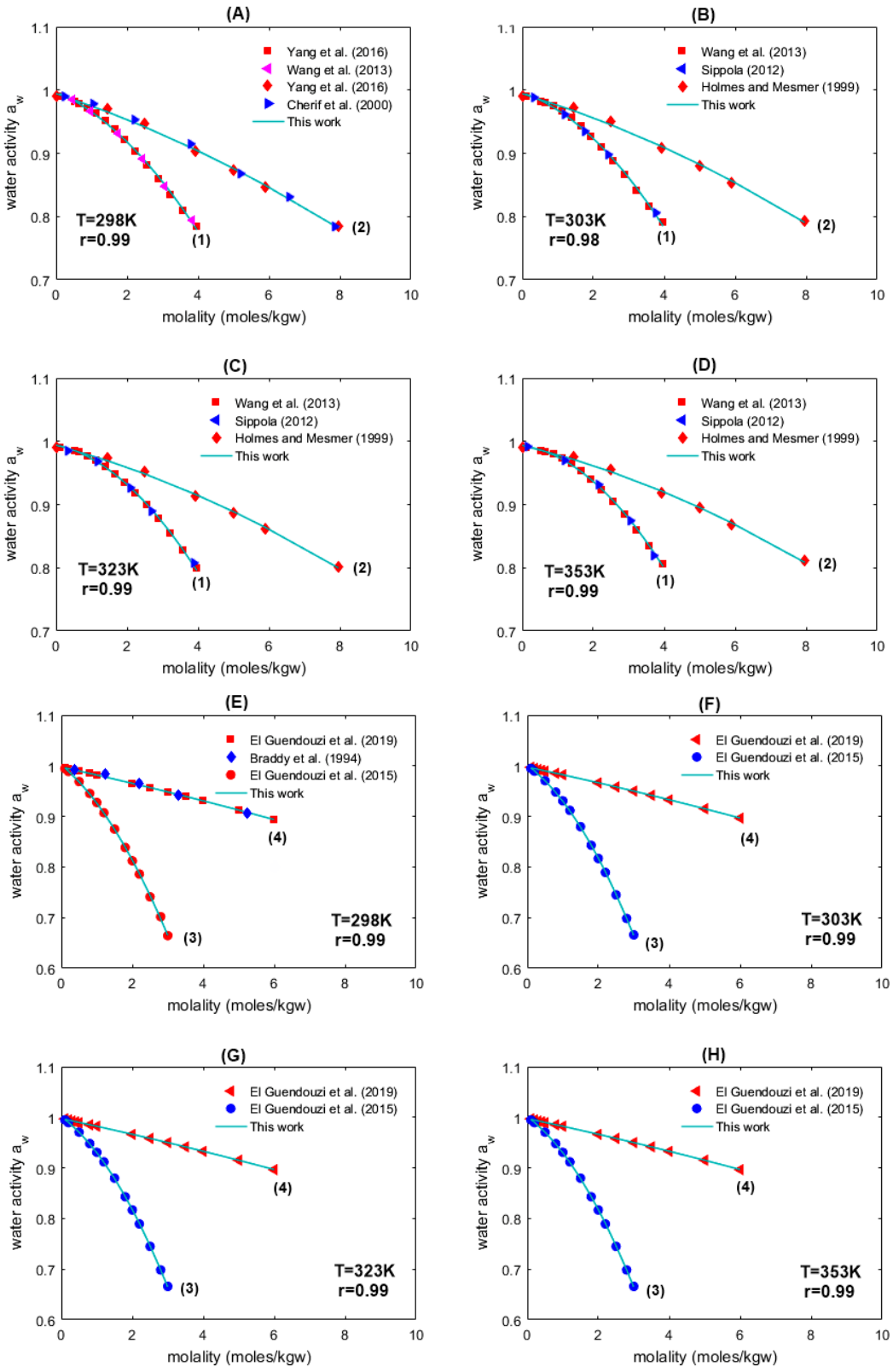

Figure 5: Model vs measurements. (A-H): water in different systems. (1: $H_2SO_4 - H_2O$, 2: $H_3PO_4 - H_2O$, 3: $H_2SiF_6 - H_2O$, 4: $HF - H_2O$).

4. Results and discussion

The results of the estimability analysis provided the most estimable parameters to be identified through the minimization of the mean-square error (Eq.26) between the available experiments and the predictions of the model. The values of the identified parameters are listed in Table 3 along with their confidence intervals. It is worth mentioning that parameters without interval confidence are not estimable, and their values are taken from previous works or from the literature. These parameters are then used to compare the predictions of the developed model to the available measurements. The results are presented in Figs. 3A-H, 4A-H and 5A-H. To assess the accuracy of the model predictions, the Pearson product-moment coefficient r is also computed in each case. Its high values highlight the accuracy and the reliability of the model. The latter is then exploited in the multi-objective optimization problem to predict the values of the objective functions. The ϵ-constraint method (Deb, 2014) is used to transform the multi-objective optimization problem to a single-objective optimization problem which is then solved several times accurately by means of a global optimization solver to determine the Pareto front of optimal solutions.

4.1. Pareto front

The multi-objective optimization problem is formulated as the following single-objective optimization problem:

$$
\begin{aligned}
Max_x \quad & -f_1(x) & \\
\text{subject to} \quad & f_2(x) \geq \epsilon & \\
& g_j(x) = 0 & j \in [1; J] \\
& h_k(x) \geq 0 & k \in [1; K] \\
& x_i^{(L)} \leq x_i \leq x_i^{(U)} & i \in [1; N]
\end{aligned}
$$

where f_1 and f_2 are the two conflicting objectives predicted using the developed thermodynamic model, x is the vector of decision variables, i.e., $[w_1, w_2, w_3, S_c, Q_{cool}]$, $x^{(L)}$ and $x^{(U)}$ their lower and upper bounds. $g = (g_1, g_2, ..., g_J)^T$ and J are the equality constraints and their number respectively, $h = (h_1, h_2, ..., h_K)^T$ and K refer to the inequality constraints and their number.

The epsilon-constraint optimization problem is then implemented and solved within GAMS environment. Moreover, a branch-and-reduce algorithm (Belotti et al., 2009; Sahinidis, 2002) is used to solve the problem to global optimality. It should be noted that the method has the advantage of finding any Pareto optimal solution, even for non-convex problems. However, it is not always easy to set the lower limit ϵ so that the problem has feasible solutions.

The Pareto front computed is presented in Fig.6 and shows that (i) the saturation index of brushite (syncristallized losses) is negative for all the optimal solutions meaning that the thermodynamic conditions are not favorable for its production, (ii) the saturation index of gypsum is positive with higher values for all the optimal solutions meaning that the thermodynamic conditions are very favorable for its production and consequently for increasing the productivity of the industrial unit.

On the other hand, solutions are taken from the Pareto front and detailed in Table 4. They show that the optimal distribution of sulfuric acid in the three sections varies between 63% and 73% (w_1) for the first section, between 27% and 37% (w_2) for the second and 0% (w_3) for the last section. These values are very consistent with the current distributions used on industrial scale, in particular within a phosphoric acid plant located in Jorf Lasfar in Morocco (Bouchkira and El Fariq, 2017; El Bouzidi, 2016).

Furthermore, the excess of sulfuric acid (with respect to the stoichiometric amount) lies between 2% and 3%, which is in good agreement on the one hand with the current operating conditions of the industrial units, and on the other hand with the conditions favorable to the crystallization of gypsum described by Becker (1989) . It is noteworthy that the optimal solutions for sulfuric acid distributions are not uniform. In fact, as the conversion rate of the digestion increases from the first to the last section, the demand for sulfuric acid varies in the opposite direction and decreases from the first to the third section. Optimal temperatures are also reported in Table 4, their values allow to determine the overall heat quantity to be removed via the flash cooler to ensure good conditions for gypsum crystallization and also to limit the formation of bassanite which undermines the quality of the filtration unit downstream of the digestion tank.

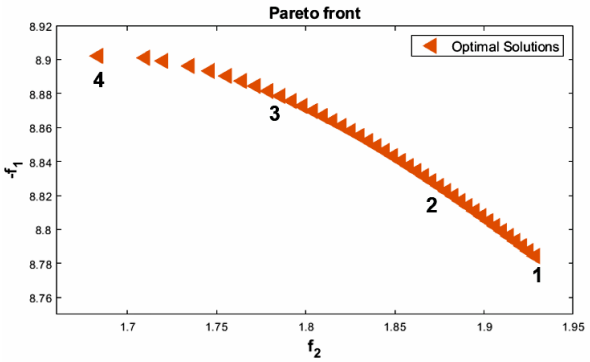

Figure 6: Pareto front of the optimization problem with four points enumerated 1-4 and reported in Table 4.

Table 4: Four solutions from the Pareto front

	w_1	w_2	w_3	$T^{opt}(°C)$	$S_c(\%)$	$Q_{cool}(kJ/hr)$
1	0.73	0.27	0	76.3	2.12%	-1.333. 10^5
2	0.70	0.30	0	77.1	2.18%	-1.351. 10^5
3	0.67	0.33	0	77.6	2.23%	-1.355. 10^5
4	0.63	0.37	0	78.2	2.54%	-1.358. 10^5

4.2. Decision-making aid method

Once the Pareto front is determined, the issue is to rate and rank all the optimal solutions in order to select the best one to be implemented. A multi-objective decision-making aid method is therefore needed. The decision aid method used in this work is the multi attribute-utility theory (Mateo, 2012). It is mainly based on the calculation of individual utility functions (denoted by u_1 and u_2) of each objective function and then to use them to rank the optimal solutions through the calculation of a multi-attribute utility function noted U.

$$u_1(x) = \left(\frac{f_1^{max} - f_1(x)}{f_1^{max} - f_1^{min}} \right)^{\alpha_1} \tag{32}$$

$$u_2(x) = \left(\frac{f_2(x) - f_2^{min}}{f_2^{max} - f_2^{min}} \right)^{\alpha_2} \tag{33}$$

f_1^{max} and f_2^{max} are the maximum values of the objectives of the Pareto front and f_1^{min} and f_2^{min} are their minimum values. α_1 and α_2 are related to the relative tolerance on the individual utility functions. The multi-attribute utility function is defined as:

$$U(x) = w_1.u_1(x) + w_2.u_2(x) \tag{34}$$

where w_1 and w_2 are usually set by a decision-maker according to his/her preferences. They express the weight of each objective in the decision. The values of the multi-attribute utility function allow then to rank the optimal solutions and consequently to select the best one to be implemented.

Figs 7A-B show the effect of the relative tolerances α_1 and α_2 on the individual utility functions. They represent the sensitivity of u_1 and u_2 with respect to f_1 and f_2. Their values are set in our case to $\alpha_1 = 0.5$ and $\alpha_2 = 0.5$. Meanwhile, the values of the weighting parameters w_1 and w_2 are taken equal to 0.5 to consider that the two objective functions have the same importance in the optimization problem.

The individual utility function $U(x)$ was calculated for each point of the Pareto front and used to rank the optimal solutions. The first two best solutions are shown in Table 5 (no 9 and 10), along with experimental measurements (no 1 to 8) from (Bouchkira and El Fariq, 2017; El Bouzidi, 2016). It is important to point out that the total losses seem very small and one might be tempted to ignore them. However, the industrial phosphoric acid plant located in Jorf Lasfar in Morocco (studied in this work), includes 16 units treating 1,400 tons of phosphate ore per day each. Therefore, 1% loss corresponds to 224 tons of phosphate loss per day, which are significant and cannot be neglected.

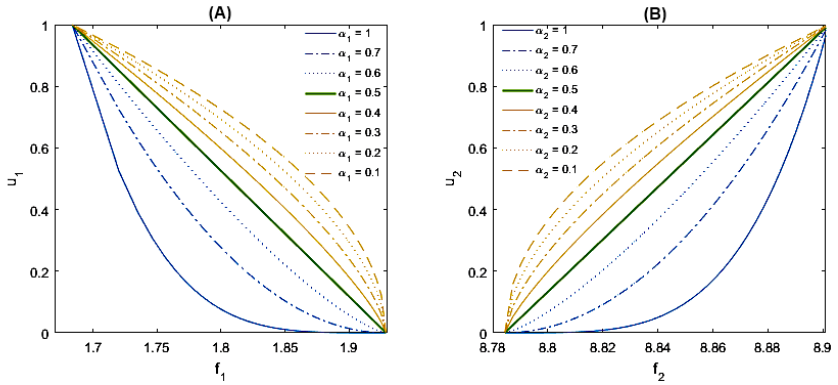

Figure 7: Relative tolerance factors α_i effect. (a) Saturation index of gypsum, (b) Saturation index of Brushite.

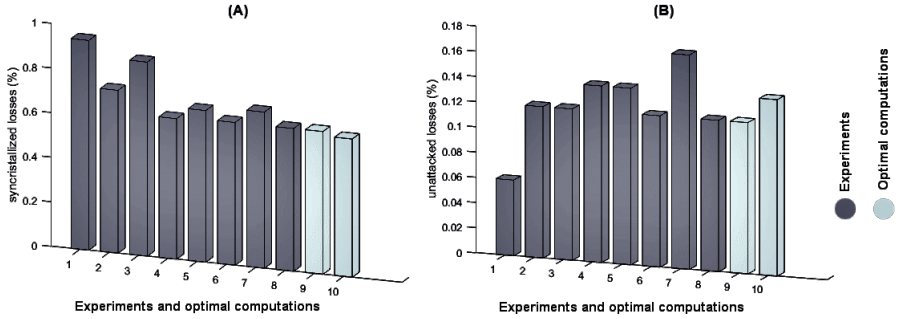

Figure 8: Chemical losses, (A): unattacked losses, (B): syncrystallized losses

Moreover, to compare the results of the implementation of these two best optimal solutions to the measurements carried out on industrial plants, a fractional design of experiments (Park, 2007) is used to develop a surrogate model in order to predict the syncrystallized as well as the unattacked losses of phosphate. Given the complexity of the process and lack of industrial measurements, two factors (i.e., temperature and excess sulfuric acid) are assumed to be known. Therefore, only three factors out of five, i.e., w_1, w_2, w_3, are considered with two levels.

The design of experiment's factors along with their levels are reported in Table 6. The surrogate model adopted is expressed as :

$$Y^{mod} = a_0 + \sum_i b_i x_i + \sum_i \sum_j c_{i,j} x_i x_j \tag{35}$$

$$\theta = (X^T.X)^{-1}.X^T.Y^{exp} \tag{36}$$

where Y^{mod} refers to the surrogate model predictions. Y^{exp} is the vector of measured values. X is the matrix of the experimental design. x_i and x_j are the levels of the three considered variables. θ is the vector of the unknown coefficients of the surrogate model given as:

$$\theta = [a_0\ b_1\ b_2\ b_3\ c_{1,2}\ c_{1,3}\ c_{2,3}]^t \tag{37}$$

Figs. 8A-B show a comparison between industrial losses taken from (Bouchkira and El Fariq, 2017; El Bouzidi, 2016) and the first two best optimal solutions. The computed solutions are very close to the industrial measurements which are obtained by performing several run-to-run on the plant by changing the values of the decision variables from one run to the next to improve the productivity and minimize the phosphate losses. Moreover, the values of the decision variables used to carry out industrial experiments, are sub-optimal and must be adjusted depending on the composition of the phosphate ore which further increases the number of runs. It is easy to understand under these conditions that obtaining these measurements is very costly since it involves significant labor cost, consumes time and huge quantities of reagents, decreases the productivity of the plant and poses some safety issues. Modeling and multi-criteria optimization have proven to be effective since they provide optimal solutions that minimize the number, duration, cost of runs, and security risks.

Table 5: Industrial measurements and optimal solutions

	w_1	w_2	w_3	$SL(\%)$	$UL(\%)$	Reference
1	0.50	0.20	0.30	0.94	0.06	El Bouzidi (2016)
2	0.40	0.20	0.40	0.73	0.12	
3	0.40	0.30	0.30	0.87	0.12	
4	0.70	0.30	0	0.62	0.14	Bouchkira and El Fariq (2017)
5	0.64	0.36	0	0.70	0.15	
6	0.75	0.25	0	0.64	0.12	
7	0.75	0.17	0.08	0.68	0.14	
8	0.60	0.30	0.10	0.63	0.12	
9	0.65	0.35	0	0.64	0.12	This work
10	0.63	0.37	0	0.62	0.14	

Table 6: Design of experiments levels: $L_{(+1)}$ and $L_{(-1)}$. SL and UL refer to syncristallized and unattacked losses.

	w_1	w_2	w_3	$SL(\%)$	$UL(\%)$
1	+1	+1	-1	0.62	0.14
2	+1	-1	-1	0.64	0.12
3	-1	-1	+1	0.94	0.06
4	-1	+1	+1	0.87	0.12
$L_{(+1)}$	[0.5;0.7]	[0.2;0.3]	[0.2;0.4]	-	-
$L_{(-1)}$	[0.4;0.5]	[0.1;0.2]	[0; 0.2]	-	-

5. Conclusion

Optimal operating conditions of the digestion tank of an industrial phosphoric acid production process are determined by means of a multi-objective optimization method. The objectives used (i.e., saturation indices) have proven to be effective in minimizing the phosphate losses and increasing the acid productivity. Furthermore, the two inequality constraints on the temperature and on the excess of sulfuric acid above the stoichiometric amount required by the reactions were relevant to ensure an optimal operation of the digestion tank.

The optimization results are consistent with the measurements carried out on an industrial plant, thus showing that optimization is a powerful tool for reducing the cost and duration of industrial experiments under maximum safety conditions.

However, it is noteworthy that some side reactions can occur due to the impurities present in the phosphate ore which are not taken into account in this work. Their consideration in future works would undoubtedly improve the performance of the digestion tank.

Declaration of Competing Interest

The authors declare that they have no known competing financial interests or personal relationships that could have appeared to influence the work reported in this paper.

Acknowlgedgments

The authors are grateful to OCP Group for its financial support.

References

Amin, M., Ali, M., Kamal, H., Youssef, A., & Akl, M. (2010). Recovery of high grade phosphoric acid from wet process acid by solvent extraction with aliphatic alcohols. *Hydrometallurgy*, *105*(1-2), 115–119. https://doi.org/10.1016/j.hydromet.2010.08.007

Azimi, G., & Papangelakis, V. (2010). The solubility of gypsum and anhydrite in simulated laterite pressure acid leach solutions up to 250 c. *Hydrometallurgy*, *102*(1-4), 1–13. https://doi.org/10.1016/j.hydromet.2009.12.009

Ball, J. W., & Nordstrom, D. K. (1991). Wateq4f–user's manual with revised thermodynamic data base and test cases for calculating speciation of major, trace and redox elements in natural waters.

Becker, P. (1989). Phosphates and phosphoric acid: Raw materials, technology, and economics of the wet process. *Marcel Dekker, Inc.*, *6*.

Belotti, P., Lee, J., Liberti, L., Margot, F., & Wächter, A. (2009). Branching and bounds tighteningtechniques for non-convex minlp. *Optimization Methods & Software*, *24*(4-5), 597–634. https://doi.org/10.1080/10556780903087124

Bouchkira, I., & El Fariq, Y. (2017). Improvement of the 28 % phosphoric acid production units. *MSc thesis, ENSA, Khouribga, Morocco*.

Bouchkira, I., Latifi, A. M., Khamar, L., & Benjelloun, S. (2021). Global sensitivity based estimability analysis for the parameter identification of pitzer's thermodynamic model. *Reliability Engineering & System Safety*, *207*, 107263. https://doi.org/10.1016/j.ress.2020.107263

Braddy, R., McTigue, P., & Verity, B. (1994). Equilibria in moderately concentrated aqueous hydrogen fluoride solutions. *Journal of Fluorine Chemistry*, *66*(1), 63–67. https://doi.org/10.1016/0022-1139(93)02895-L

Cherif, M., Mgaidi, A., Ammar, M. N., Abderrabba, M., & Fürst, W. (2000). Modelling of the equilibrium properties of the system h3po4–h2o: Representation of vle and liquid phase composition. *Fluid Phase Equilibria*, *175*(1-2), 197–212. https://doi.org/10.1016/S0378-3812(00)00458-1

Chidambaram, S., Karmegam, U., Sasidhar, P., Prasanna, M. V., Manivannan, R., Arunachalam, S., Manikandan, S., & Anandhan, P. (2011). Significance of saturation index of certain clay minerals in shallow coastal groundwater, in and around kalpakkam, tamil nadu, india. *Journal of Earth System Science*, *120*(5), 897–909. https://doi.org/10.1007/s12040-011-0105-2

Christov, C., & Moller, N. (2004). Chemical equilibrium model of solution behavior and solubility in the h-na-k-oh-cl-hso4-so4-h2o system to high concentration and temperature. *Geochimica et Cosmochimica Acta*, *68*(6), 1309–1331. https://doi.org/10.1016/j.gca.2003.08.017

Deb, K. (2014). Multi-objective optimization. search methodologies. *Search Methodologies. New York: Springer*.

Dorozhkin, S. V. (1996). Fundamentals of the wet-process phosphoric acid production. 1. kinetics and mechanism of the phosphate rock dissolution. *Industrial & Engineering Chemistry Eesearch*, *35*(11), 4328–4335. https://doi.org/10.1021/ie960092u

Dutrizac, J. (2002). Calcium sulphate solubilities in simulated zinc processing solutions. *Hydrometallurgy*, *65*(2-3), 109–135. https://doi.org/10.1016/S0304-386X(02)00082-8

El Bouzidi, S. (2016). Improvement of two phosphoric acid units. *MSc thesis, ENSA, Khouribga, Morocco*.

El Guendouzi, M., Faridi, J., & Khamar, L. (2019). Chemical speciation of aqueous hydrogen fluoride at various temperatures from 298.15 k to 353.15 k. *Fluid Phase Equilibria*, *499*, 112244. https://doi.org/doi.org/10.1016/j.fluid.2019.112244

Elmore, K., Hatfield, J., Dunn, R., & Jones, A. (1965). Dissociation of phosphoric acid solutions at 25. *The Journal of Physical Chemistry*, *69*(10), 3520–3525. https://doi.org/10.1021/j100894a045

Geeson, M. B., & Cummins, C. C. (2018). Phosphoric acid as a precursor to chemicals traditionally synthesized from white phosphorus. *Science*, *359*(6382), 1383–1385. https://doi.org/10.1126/science.aar6620

Gustafsson, J. P. (2011). Visual minteq 3.0 user guide. *KTH, Department of Land and Water Recources, Stockholm, Sweden*.

Holmes, H., & Mesmer, R. (1999). Isopiestic studies of h3po4 (aq) at elevated temperatures. *Journal of Solution Chemistry*, *28*(4), 327–340. https://doi.org/10.1023/A:1022651710922

Irish, D., & Chen, H. (1971). Raman spectral study of bisulfate-sulfate systems. ii. constitution, equilibriums, and ultrafast proton transfer in sulfuric acid. *The Journal of Physical Chemistry*, *75*(17), 2672–2681. https://doi.org/10.1021/j100686a024

Keith, T. Z. (2014). *Multiple regression and beyond: An introduction to multiple regression and structural equation modeling*. Routledge.

Lampila, L. E. (2013). Applications and functions of food-grade phosphates. *Annals of the New York Academy of Sciences*, *1301*(1), 37–44.

Langman, M. (1986). Towards estimation and confidence intervals. *British Medical Journal*, *292*(6522), 716. https://doi.org/10.1136/bmj.292.6522.716

Leikam, D. F., & Achorn, F. P. (2005). Phosphate fertilizers: Production, characteristics, and technologies. *Phosphorus: Agriculture and the Environment*, *46*, 23–50. https://doi.org/10.2134/agronmonogr46.c2

Li, R., Wang, J. J., Zhou, B., Awasthi, M. K., Ali, A., Zhang, Z., Lahori, A. H., & Mahar, A. (2016). Recovery of phosphate from aqueous solution by magnesium oxide decorated magnetic biochar and its potential as phosphate-based fertilizer substitute. *Bioresource Technology*, *215*, 209–214. https://doi.org/10.1016/j.biortech.2016.02.125

Mateo, J. R. S. C. (2012). Multi-attribute utility theory, In *Multi criteria analysis in the renewable energy industry*. Springer. https://doi.org/10.1007/978-1-4471-2346-0_10

McCleskey, R. B., Nordstrom, D. K., Ryan, J. N., & Ball, J. W. (2012). A new method of calculating electrical conductivity with applications to natural waters. *Geochimica et Cosmochimica Acta*, *77*, 369–382. https://doi.org/10.1016/j.gca.2011.10.031

Messnaoui, B., & Bounahmidi, T. (2005). Modeling of excess properties and vapor–liquid equilibrium of the system h3po4–h2o. *Fluid Phase Equilibria*, *237*(1-2), 77–85. https://doi.org/10.1016/j.fluid.2005.08.002

Messnaoui, B., & Bounahmidi, T. (2006). On the modeling of calcium sulfate solubility in aqueous solutions. *Fluid Phase Equilibria*, *244*(2), 117–127. https://doi.org/10.1016/j.fluid.2006.03.022

Park, G.-J. (2007). Design of experiments. *Analytic Methods for Design Practice*, 309–391. https://doi.org/10.1007/978-1-84628-473-1_6

Pitzer, K. S. (2018). *Activity coefficients in electrolyte solutions*. CRC press.

Preston, C. M., & Adams, W. (1979). A laser raman spectroscopic study of aqueous orthophosphate salts. *Journal of Physical Chemistry*, *83*(7), 814–821. https://doi.org/10.1021/j100470a011

Rickard, D. A. (2000). Review of phosphorus acid and its salts as fertilizer materials. *Journal of Plant Nutrition*, *23*(2), 161–180. https://doi.org/10.1080/01904160009382006

Sahinidis, N. V. (2002). Global optimization and constraint satisfaction: The branch-and-reduce approach, In *International workshop on global optimization and constraint satisfaction*. Springer. https://doi.org/10.1007/978-3-540-39901-8_1

Shen, L., Sippola, H., Li, X., Lindberg, D., & Taskinen, P. (2020). Thermodynamic modeling of calcium sulfate hydrates in a caso4–h2so4–h2o system from 273.15 to 473.15 k up to 5 m sulfuric acid. *Journal of Chemical & Engineering Data*, *65*(5), 2310–2324. https://doi.org/10.1021/acs.jced.9b00829

Simoes, M. C., Hughes, K. J., Ingham, D. B., Ma, L., & Pourkashanian, M. (2017). Temperature dependence of the parameters in the pitzer equations. *Journal of Chemical & Engineering Data*, *62*(7), 2000–2013. https://doi.org/10.1021/acs.jced.7b00022

Sippola, H. (2012). Thermodynamic modelling of concentrated sulfuric acid solutions. *Calphad*, *38*, 168–176. https://doi.org/10.1016/j.calphad.2012.06.008

Sippola, H., & Taskinen, P. (2014). Thermodynamic properties of aqueous sulfuric acid. *Journal of Chemical & Engineering Data*, *59*(8), 2389–2407. https://doi.org/10.1021/je4011147

Slack, A. (1968). *Fertilizer science and technology series* (Vol. 1). Marcel Dekker.

Slack, A., & James, G. (1973). Ammonia. fertilizer science and technology series. marcel deckker. *Inc. New York*.

Wang, W., Zeng, D., Chen, Q., & Yin, X. (2013). Experimental determination and modeling of gypsum and insoluble anhydrite solubility in the system caso4–h2so4–h2o. *Chemical Engineering Science*, *101*, 120–129. https://doi.org/10.1016/j.ces.2013.06.023

Yang, H., Zhao, Z., Zeng, D., & Yin, R. (2016). Isopiestic measurements of water activity for the h2so4–h3po4–h2o system at 298.15 k. *Journal of Solution Chemistry*, *45*(11), 1580–1587. https://doi.org/10.1007/s10953-016-0516-4

Zdanovskii, A., & Vlasov, G. (1968). Determination of the boundaries of the reciprocal transformation of caso4. 2h2o and γ-caso4 in h2so4 solutions. *Russian Journal of Inorganic Chemistry*, *13*, 1318–1319.